Research on the Possible Application of Polyolefin Waste-Derived Pyrolysis Oils for ANFO Manufacturing

Andrzej Biessikirski [1,*] , **Dominik Czerwonka** [2], **Jolanta Biegańska** [1], **Łukasz Kuterasiński** [3] ,
Magdalena Ziąbka [4] , **Michał Dworzak** [1] and **Michał Twardosz** [1]

1   Faculty of Mining and Geoengineering, AGH University of Science and Technology, Al. Mickiewicza 30,
    30-059 Kraków, Poland; biega@agh.edu.pl (J.B.); dworzak@agh.edu.pl (M.D.); michaltw@agh.edu.pl (M.T.)
2   Technology and Design, Department of Chemistry, Faculty of Materials Science, University of Technology
    and Humanities in Radom, Chrobrego 27, 26-600 Radom, Poland; dominikczerwonka@tlen.pl
3   Jerzy Haber Institute of Catalysis and Surface Chemistry, Polish Academy of Sciences, ul. Niezapominajek 8,
    30-239 Kraków, Poland; nckutera@cyf-kr.edu.pl
4   Faculty of Materials Science and Ceramics, AGH University of Science and Technology, Al. Mickiewicza 30,
    30-059 Kraków, Poland; ziabka@agh.edu.pl
*   Correspondence: abiess@agh.edu.pl; Tel.: +48-12-67-36-39

Abstract: This work aims to evaluate the possible application of pyrolysis fuel oils obtained through the pyrolysis of waste plastics. by comparing both the blasting properties and morphology results of Ammonium Nitrate Fuel Oil (ANFO), which is applied in the mining industry, and ANFO based on pyrolysis fuel oils (FOs), as well as low-temperature properties of all tested FO samples. The low-temperature research includes the measurements of density, kinematic viscosity, flash point, pour point, and cloud point. Moreover, a stability analysis was carried out based on the Turbiscan Stability Index (TSI) coefficient. Based on the obtained results it was concluded that despite pyrolysis FOs showing some differences in comparison with index FO, none of their properties indicated that pyrolysis FOs should be excluded from possible application in ANFO. Additionally, IR, XRD, and SEM analyses were conducted for all ANFO samples. The instrumental analysis did not show any dribbling effect. The blasting tests such as velocity of detonation (VOD), the heat of explosion, and post-blast fumes revealed that VOD values were lower in comparison to the reference ANFO sample. However, the observed differences were either negligible (heat of explosion) or small enough (VOD) to conclude that polyolefin waste-derived pyrolysis fuel oils can be applied as ANFO's fuel component.

1. Introduction

Ammonium Nitrate Fuel Oil (ANFO) is a non-ideal explosive most frequently obtained by mixing ammonium nitrate (V) with a volatile component (usually fuel oil (FO)), in an appropriate weight ratio (most often 94.5:5.5) that guarantees a zero oxygen balance. In the case of the mining industry, ammonium nitrate (V) porous prill (AN-PP) is applied. This is recommended, since in comparison to fertilizer grade ammonium nitrate (AN_F), AN-PP has a lower density, a higher retention, and a higher absorption index, ranging from 12% to 16% (in the case of AN-F it is ca. 8%), which impacts the detonation reaction [1–3]. Moreover, Landucci et al. concluded that ammonium nitrate (V), which is applied in the mining industry, has a 20% void fraction and is much more energy-efficient [4]. However, AN-PP is highly soluble in water, which limits ANFO application in dry boreholes in open-strip mining. Despite this fact, ANFO remains one of the most commonly used explosives in mining globally [5], due to the simplicity of production, high accessibility of products required for its production, low cost of production, and numerous ways of adjusting its explosive properties.

Miyake et al. defined ANFO as a non-ideal explosive material due to the fact that it was impossible to reach the theoretically determined detonation velocity [6]. This was confirmed by Maranda's research [7] on determining the detonation velocity, critical diameter, and ability to carry out work using ammonium nitrate-based materials, as well as the detonation models developed by Nazarian and Presser, Paszula and Kowalski, Trzciński and Haque-Pawlik, and Hang and Chang [8–11].

The proper selection of the oxide component for the manufacturing of ANFO is widely discussed in numerous studies [3,5,12–15]. On the basis of the conducted research into the ANFO morphological and blasting properties, it was determined that ammonium nitrate (V) porous prill (AN-PP) is the recommended oxide component. This was justified by the presence of numerous surface deformations, and the presence of micro- and macropores on the surface of the granule, which increases the contact surface between the flammable component and ammonium nitrate (V), thus improving the blasting properties [14,15].

The applicability of various flammable components was investigated in the referenced papers [16,17]. Sinditskii el al. found that the content of charcoal, 2,4,6-trinitrotoluene, fuel oil (FO), or iron persulfide (II) as the flammable component is indispensable for the explosive transformation to occur [16,17]. Gunawan and Zhang noticed that the presence of pyrite in the chemical composition of ANFO additionally catalyzes the decomposition reaction of an explosive [17]. The influence of the flammable component on the blasting properties of ANFO was studied in the following work [18–22]. In these studies, the combustible components were as follows—coal dust, sugar in powdered and crystalline forms as well as aluminum dust, 2,4,6-trinitrotoluene, and fuel oil. The applicability of waste products from the process of glycol distillation as a flammable component was also the subject of a patent [23]. Biessikirski et al. investigated the applicability of various flammable components, including re-use fuel oils obtained through the pyrolysis of tires and hydraulic machinery drives, in the manufacturing of non-ideal explosives [24]. Ucar et al. and Sipra et al. noticed that the application of pyrolysis as a method for the chemical recycling of plastic-based oils is likely to become one of the approaches to rational waste management [25,26]. The possibility of using catalytic processing of used oils and oil residues [27], used car oils [28], lubricant products [29], as well as polyolefin wastes [30–32], with the aim of obtaining a high-quality liquid or gaseous fuels is broadly discussed in the relevant literature. These studies confirmed [33–39] the high potential of the pyrolysis of wastes as a method for producing fuels. Kalargaris et al. researched the possible application of plastic pyrolysis oils blends made at 900 °C with diesel oil. They stated that a non-blended oil would not be suitable for long-running activity, due to the more extended ignition period. The only way to utilize non-blended fuel oil is to increase the blending ratio with diesel oils [37–39].

On the other hand, Owusu et al. stated that according to laboratory tests, the characteristics of the high-density polyethene (HDPE) and polypropylene (PP) fuel oil samples were similar to the characteristics of conventional fuel oil [40]. Waste polyolefins are free of oxygen and possess a high hydrogen content. This might lead to obtaining FO of limited applicability, in comparison to conventionally obtained types of gasoline or fuel oils [41–43].

This paper aims to present the possible application of pyrolysis fuel oils obtained through the pyrolysis of various plastics into ANFO. Based on the reference analysis, it was observed that some general research was conducted, however, it mostly focused on waste vegetable FO. Moreover, the obtained results were published only in a limited manner. Our research indicates that pyrolysis fuel oils obtained through the pyrolysis of plastics could be applied in the mining industry, once some additional post-processing is performed. The new possible application of waste plastic might also influence general waste management.

2. Materials and Methods

2.1. Materials

In the conducted research, five different fuel oil samples (P1–P5) obtained as a result of the process of catalytic cracking of polyethene (PE)-, polypropylene (PP)-, and polystyrene (PS)-based waste polyolefins were investigated. The detailed chemical composition of the pyrolysis FOs is presented in Table 1.

Table 1. The low-temperature properties of the tested oils.

Parameters	FO Sample				
	P1	**P2**	**P3**	**P4**	**P5**
Aliphatic hydrocarbons, %	27	25.8	28.8	28	25.3
Cyclic aliphatic hydrocarbons, %	4.2	5.1	4.8	5.4	4.3
Aromatic hydrocarbons, %	30.9	33.2	30.7	31.8	31.9
Cyclic aliphatic/aromatic compounds hydrocarbons, %	9.3	8.1	10.3	9.8	8.7
Cycloalkene, %	7.2	8.3	9.4	9	12.5
Diene, %	5.2	5.4	4.2	4.5	6.1
Others, %	16.2	14.1	11.8	11.5	11.2

Fuel oil, which is currently used in the manufacturing of ANFO, was used as the reference sample (P6). A detailed physiochemical characterization of the reference fuel oil is presented in [24].

AN-PP that is used in the mining industry to prepare explosive charges was manufactured by Yara Poland Sp. z o.o. The product purity amounted to 99.5%. The nitrogen content was determined to be 35.0%. The grain-size range was 1–2 mm, while the density of ammonium nitrate was 0.82 g·cm^{-3}. The moisture content did not exceed 0.3%. AN-PP samples were derived from the batch produced in 2019.

2.2. Methods

2.2.1. Plastic Pyrolysis FO and Non-Ideal Explosives

The P1–P5 FO samples (containing post-pyrolysis fuel oil) were obtained in the EKON-AKS installation in Skarżysko Kamienna. The obtained fuel oils were based on the company's own solutions included in a patent application that enabled industrial-scale manufacturing.

Pulverized plastic was continuously fed into the reactor in the form of a mixture including 70–80% PE, 10–30% PP, and 0–10% PS. Catalytic cracking of long hydrocarbon chains was performed at a temperature of 380–460 °C, in the presence of ultra-stabilized zeolite with a faujasite structure or illite aluminosilicates with a smectite structure. The vaporous or gaseous products formed as a result of catalytic cracking were passed to the cooling assembly to make them condense. Next, the products passed to the titration unit, from where they were pumped to the main vessel. The average pyrolysis reaction efficiency amounted to approximately 80%. Due to its high hydrocarbon content of >C15, the broad fraction that was obtained through pyrolysis was broken down under laboratory conditions, through atmospheric distillation. The obtained P1–P5 FO samples represented the removed fraction with a boiling point of 130–320 °C. As it was impossible to determine a stable chemical composition (inability to interfere with the manufacturing process), the fuel oil samples were taken from five different manufactured batches.

The samples of non-ideal explosives were prepared by mixing AN-PP with FO in a mass ratio of 94:6. AN-PP was mixed with FO for 20 min at 250 rpm, using a laboratory mixer.

2.2.2. Measurements of Low-Temperature Properties

The fuel oil density was researched using a glass pycnometer whose capacity was determined by a measurement performed for distilled water. The weighed pycnometer was filled with the tested fuel–oil at a temperature similar to the experimental temperature

(20 °C). Next, the pycnometer was placed in a water bath kept at 20 °C for 30 min [44]. The density of the tested fuel oil was calculated from (1).

$$d_{20} = \frac{m_3 - m_1}{m_2 - m_1} \tag{1}$$

where d_{20} denotes the density at 20 °C, g·cm^3; m_1—the mass of the empty pycnometer, g; m_2—the mass of the pycnometer filled with water, g; m_3—the mass of the pycnometer with the tested liquid, g. The determined density values are presented in Table 2.

Table 2. The low-temperature properties of the tested oils.

Parameters	FO Sample					
	P1	**P2**	**P3**	**P4**	**P5**	**P6**
Density at 20 °C, (d) kg·m^{-3}	805.6	801.3	801.7	800.6	803.1	873.2 ±1.2
Kinematic density at 40 °C, (ν) mm^2·s^{-1}	1.99	1.95	1.93	1.93	1.98	13.6 ±0.0
Flash point, °C	62.1 ±0.9	61.3 ±0.8	59.4 ±1.2	62.2 ±0.8	62 ±1.1	127.3 ±1.2
Cloud point (CP), °C	3 ±2.0	3 ±2.0	2 ±2.0	2 ±2.0	3 ±2.0	8.9 ±1.1
Pour point (PP), °C	−8 ±2.0	−8 ±2.0	−9 ±2.0	−9 ±2.0	−7 ±2.0	−32 ±2.0
TSI coefficient	8.27	8.83	4.09	6.62	11.05	0.56

The kinematic density was determined using an Ubbelholde viscometer at a temperature of 40 °C [45]. The test consisted of measuring the time of the outflow of a fixed volume of liquid under the influence of gravitational forces, through the capillary of a calibrated glass viscometer. The measurement result was the product of the outflow time and the reference value of the vein. The determined viscosity values are presented in Table 2.

The CP (cloud point) was analyzed in compliance with the relevant norm [46], using a Phase Xi apparatus (Phase Technology). A sample with a volume of 159 μL was introduced onto the surface of a mirror placed at the bottom part of the measurement chamber. The measurement consisted in registering the intensity of a light ray directed at the surface of the sample, reflected from the mirror, and impinging on the optical detector. The temperature of the mirror with the sample was linearly lowered. When a sufficient level of the dew point was achieved, which manifested itself as an increase in scattering light intensity, the sample was heated until the dew point disappeared. The temperature at which the sample lost its transparency during the next cooling cycle (accompanied by a slower temperature drop) was assumed as the cloud point. The determined CP values are presented in Table 2.

The PP (pour point) is defined as the lowest temperature at which the fluidity of the tested product can be observed. While the product was cooled under the conditions defined by the norm [47], the PP was determined by placing the product in a test tube plugged with a rubber stopper that was equipped with a thermometer cooled with a cryostat. The assessment of the liquid fluidity was performed every 3 °C, while cooling the test tube by tilting it to a horizontal position. The determined PP values are presented in Table 2.

The flashpoint was determined based on the standard [48] by correlating it with the Pensky-Martens test [49]. The measurements were conducted using an automatic EraFLASH apparatus (Eralytics) with the continuously closed cup flash point method.

The flashpoint was determined by measuring the pressure inside a closed crucible (a sudden increase in the pressure caused by an explosion signaled that the flashpoint was reached). A sample with a volume of 2 cm^3 was placed in a metal crucible with a magnetic stirrer. Upon closing the measuring chamber, the contents of the crucible were heated and

stirred, simultaneously providing an electric spark every 1 °C, with electrodes located over the surface of the liquid, until the fuel vapors detonated. The determined flash point values are presented in Table 1.

The analysis of the stability of the samples characterized by a wide range of concentration and particle size was conducted using a TurbiscanClassic device. The measurement consisted of analyzing the light intensity passing along the sample and backscattered at every 20 microns. The stability of the samples was estimated by means of determining the TSI coefficient (Figure 1), calculated by summing up the changes in the transmission of light backscattering during successive measurements of the function of the sample height, in accordance with (2):

$$\text{TSI} = \sqrt{\frac{\sum_{i=0}^{n}(x_i - x_{BS})^2}{n-1}} \tag{2}$$

where x_i denotes the average backscattering for each minute of the measurement, x_{BS} is the average x_i, and n is the number of performed scans. TSI coefficient takes the values from 1 to 100. A sudden increase of TSI index indicates abrupt changes in the FO sample. Determined values of the TSI global, describing the changes that were presented in the whole sample volume are presented in Table 2.

2.2.3. Instrumental Analysis

The structural analyses of the powdered samples were conducted with a Nicolet iS10 spectrometer (Thermo Scientific, Waltham, MA, USA) equipped with an MCT detector and an attachment for measurements, using the Attenuated Total Reflectance method (ATR). The absorption of the radiation was recorded over the spectrum range of 400–650 cm^{-1}. The number of performed scans was 32 at a resolution of 4 cm^{-1}. As a result of the experiment, the spectra presented in Table 3 were obtained.

Table 3. The results of an IR analysis of AN-PP and non-ideal explosives obtained by mixing AN-PP with a FO: P1–P6.

Sample	Band, cm^{-1}									
	3240	3060	2921	2854	1755	1410	1290	1041	827	714
AN-PP	+	+	−	−	+	+	+	+	+	+
AN-PP + FO1	+	+	+	+	+	+	+	+	+	+
AN-PP + FO2	+	+	+	+	+	+	+	+	+	+
AN-PP + FO3	+	+	+	+	+	+	+	+	+	+
AN-PP + FO4	+	+	+	+	+	+	+	+	+	+
AN-PP + FO5	+	+	+	+	+	+	+	+	+	+
AN-PP + FO6	+	+	−	−	+	+	−	−	+	−

The X-ray Diffraction (XRD) measurements were conducted at room temperature, in a PANalytical X'Pert PRO MPD calorimeter (CuKα, λ = 0.1544 nm, 40 kV, 30 mA), within the angle 2θ of 2–50°, with a time-measurement step of 0.033°. The total measurement time of a single sample was 12 min. The samples in the form of powder were prepared in an agate mortar. As a result of the experiment, the diffraction patterns presented in Figure 2 were obtained.

In the analyses of the morphology of the crystals, a Nova NanoSem 200 scanning electron microscope (FEI) was used, which enabled conducting the tests under low or high vacuum. The microscope observations were carried out under low vacuum (60 Pa) using an LVD (Low Vacuum Detector) operating in the secondary electrons mode SE. The voltage of electron acceleration was 10 keV. Magnifications in the range of 200–3000 times were used. Prior to the measurements, in order to ensure the conductivity of the tested materials, the samples were bonded to test benches using a carbon conductive tape, and they were sprayed with a protective carbon layer in a Unitra Unima sputter coater. The results of the SEM observations are presented only for a selected magnification (350χ) in Figure 3.

2.2.4. Measurements of Blasting Properties

Measurements of the heat of explosives were performed in a spherical bomb calorimeter with a capacity of approximately 5.6 cm^3 and a mass of 80 kg, which was placed in a calorimetric vessel filled with distilled water. From the beginning of the measurement, the water was mixed with a propeller agitator. The water temperature was measured using a thermocouple and recorded in the device memory.

$$Q = K \cdot (\Delta T - k) \tag{3}$$

where K denotes the heat capacity of the assembly, cal. °C; ΔT—the increase in the temperature during the main period of the cycle; $\Delta T = T_3 - T_2$, °C; T_1, T_2, T_3, T_4—the characteristic temperatures of the measurement cycles, °C; k—the coefficient correcting the losses of the assembly, °C, calculated in accordance with Equation (4):

$$k = 0.5 \cdot [0.2 \cdot (T_2 - T_1) + 0.2 \cdot (T_4 - T_3)] + 0.2 \cdot (n - 1) \cdot (T_4 - T_3) \tag{4}$$

where n denotes the duration of the main period of the cycle, min.

As a result of threefold combustion of benzoic acid explosive charges under the oxygen atmosphere, the heat capacity of the calorimeter of 163,680 J·K^{-1} was obtained. The estimated heat capacity was used to determine the detonation heat of all ANFO samples. Based on the initial measurements of the detonation heat, the contribution of the primer was estimated at 41,800 J. The heat measurement was reduced by the detonation heat of the desensitized hexogen, which was equal to 5270 J·g^{-1} [50]. The combustion heat of the foil sheath was ignored due to its appreciably low value, compared to the MW detonation heat. The detonation heat of non-ideal explosives was determined by means of a two-fold detonation of the prepared explosive charges. The determined values of the detonation heat for the studied ANFO samples, apart from the P7 sample, are presented in Table 4.

Table 4. The heat of explosion of non-ideal explosives.

Sample	Energy of Explosion, J·g^{-1}		Average Energy of Explosion, J·g^{-1}	Maximum Deflection, %
	Test 1	Test 2		
AN-PP + P1	3897	4001	3950	1.3
AN-PP + P2	3781	4010	3895	2.9
AN-PP + P3	3906	4127	4020	2.7
AN-PP + P4	3797	4025	3910	2.9
AN-PP + P5	4029	3998	4010	0.4
AN-PP + P6	3923	3950	3940	0.5

The velocity of detonation (VOD) was determined according to [51]. The ANFO charge was placed in a glass tube of a 48 mm diameter. Two short circuit probes were placed throughout the top and bottom of the charge. The distance between the probes was 150 mm. The distance between the primer and top probe was equal to two charge diameters. The measurement consisted of the time difference that described the first recorded signal change on each probe. VOD was calculated according to Equation (5).

$$\text{VOD} = \frac{l}{t} \tag{5}$$

where l is the test base distance between the two probes and t is the time difference.

The 14 g RDX-based charge primed the detonation. The VOD results are presented in Table 5.

Table 5. Velocity of detonation.

Sample	Average Density, $kg \cdot m^{-3}$	Average VOD, $m \cdot s^{-1}$
AN-PP + P1	835	2550
AN-PP + P2	833	2510
AN-PP + P3	837	2590
AN-PP + P4	834	2530
AN-PP + P5	836	2580
AN-PP + P6	837	3140

3. Results and Discussion

3.1. The Low-Temperature Properties of the Tested Fuel Oils

All FO samples were subjected to low-temperature analysis in order to make a comparison of the FO samples derived from the plastic pyrolysis and the index FO (P6). This would enable performing a preliminary verification of the P1–P5 FO sample in terms of possessing low-temperature properties, which could exclude FO samples from possible application in the explosives industry. The measured low-temperature properties are presented in Table 2.

The analysis of the low-temperature properties (Table 2) indicated that, although it was impossible to determine the stable chemical composition of the product, post-pyrolysis fuel oils displayed reasonably similar properties, which could be a key argument in favor of the attempts aimed at applying re-used oils as the combustible component of ANFO. The P1–P5 FO exhibited a lower flash point within the range of 59.4–62.2 °C, in comparison to the reference oil P6 (127 °C), Table 2. A low flash point poses a risk of fuel explosion during its storage. In the case of both oils obtained through pyrolysis and the currently utilized reference oil, low cloud points were obtained—for the P1–P5 samples they were approximately 2.0–3.0 °C, whereas for the P6 sample they were 8.9 °C (Table 2). This indicates a low content of simple saturated hydrocarbons, thus preventing their easy precipitation from fuel. Such a situation could lead to further crystallization and agglomeration as a result of prolonged cooling. The pour point in the case of the P1–P5 samples exhibited higher values by approximately −9.0−−7.0 °C than in the case of the reference oil (P6) (−32 °C). This indicated a low content of long-chain hydrocarbons >C15, which was achieved by the atmospheric distillation of the post-pyrolysis fuels. On the other hand, the oil samples P1–P5 displayed more than ten times lower values of kinematic viscosity, i.e., approximately 1.93–1.99 $mm^2 \cdot s^{-1}$, in comparison to the reference sample (P6) (Table 1). The low viscosity of oil can lead to its leaking from the inside of an AN-PP granule to its surface. However, in these studies [24,52], it was demonstrated that it is possible to produce ANFO charges from the flammable components, with a kinematic viscosity of approximately 2.0 $mm^2 \cdot s^{-1}$. The obtained density results as well as kinematic density confirmed Owusu et al.'s research relating to PP (d = 0.786 $kg \cdot m^{-3}$, ν = 2.115 $mm^2 \cdot s^{-1}$), PS (d = 0.884 $kg \cdot m^{-3}$, ν = 1.461 $mm^2 \cdot s^{-1}$), and HDPE (d = 0.796 $kg \cdot m^{-3}$, ν = 2.373 $mm^2 \cdot s^{-1}$) pyrolysis oils [40].

The TSI coefficient for the P1–P5 FO sample after thirty-day storage fell within the range of ca. 4.1–11.1 (Figure 1). The most intensive changes of the parameter were observed during the first ten days of storage. They were related mainly to the sedimentation process of solid contaminants. During the next days of storage, a gradual decline in these unfavorable processes could be observed. In order to improve the stability of the tested fuels, filtering them after distillation and the addition of antioxidants seemed to be indispensable. The highest TSI coefficient was obtained for the P5 FO sample, which implied low stability. This example could result in the high content of unsaturated hydrocarbons (alkene, dienes etc.), Table 1, which were characterized by the higher reactivity and susceptibility to oxidation in comparison with saturated hydrocarbons. The reference FO sample (P6) exhibited an extremely low value of the TSI coefficient (0.56), Figure 1f, which confirmed its high stability. It should be highlighted that data gathered based on the TSI coefficient were not always sufficient and should be treated as preliminary results that determine whether a researched sample is stable.
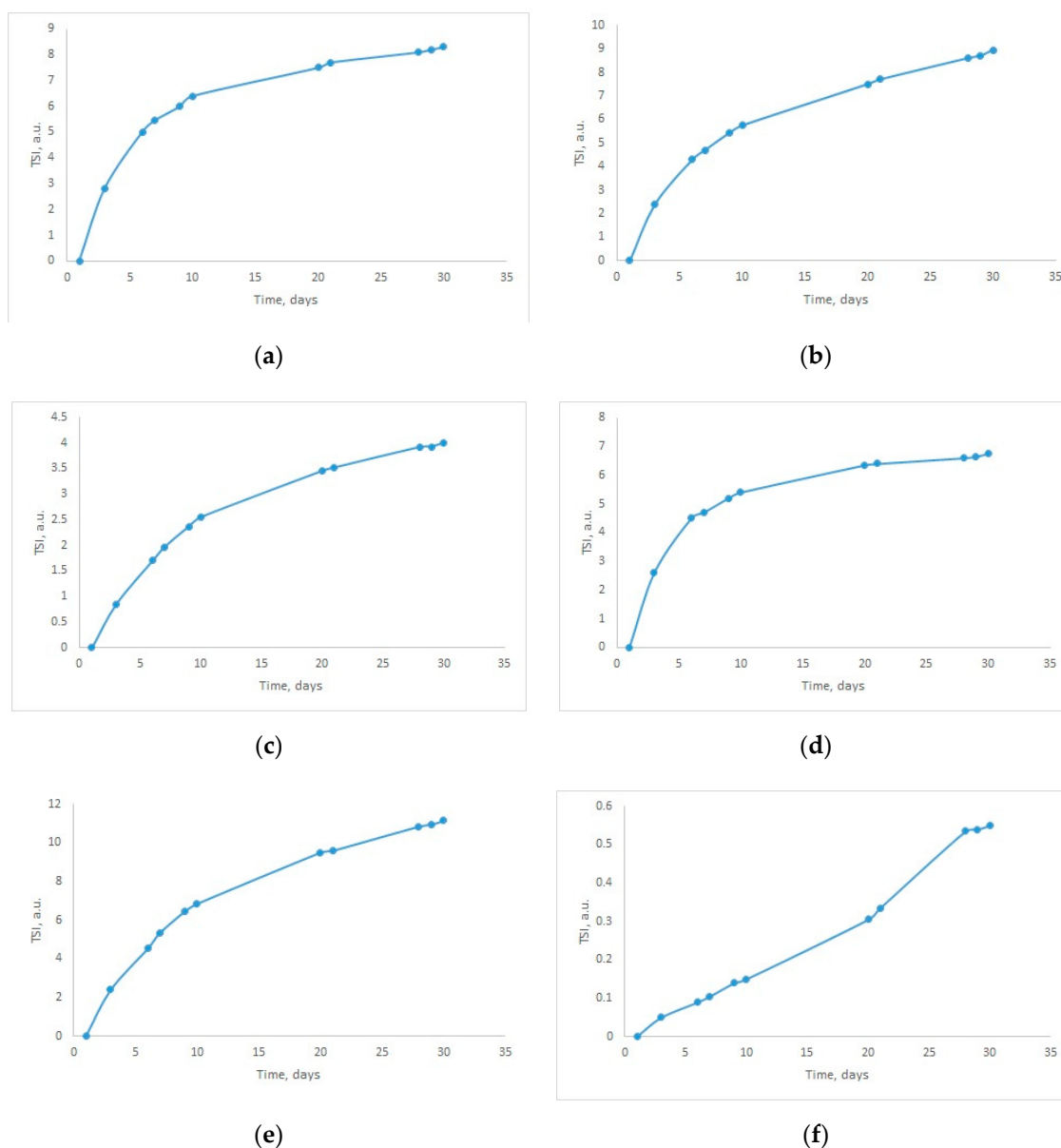
Figure 1. Stability analysis based on the TSI coefficient for the sample: (**a**) P1, (**b**) P2, (**c**) P3, (**d**) P4, (**e**) P5, and (**f**) P6.

3.2. Morphology Properties

For all samples (Table 3), the bands within the ranges of 3240 and 3060 cm^{-1} were associated with an asymmetric tensile vibrations and deformations of the ammonium cation, respectively. The presence of the 1755 cm^{-1} band might result from combinations of the tensile vibrations and in-plane deformations of the nitrate cation, or from combinations of the asymmetric deformation vibrations of the ammonium cation with the lattice vibrations. The presence of bands of approximately 1290 cm^{-1} and 1410 cm^{-1} might be related to the asymmetric deformation vibrations of NH_4^+ and the doubly degenerate plane vibrations and tensile vibrations of NO_3^- ions. The maxima of 1041 cm^{-1}, 827 cm^{-1}, and 714 cm^{-1} might reflect the symmetrical tensile vibrations, out-of-plane vibrations, and in-plane deformation vibrations of the NO_3^- ions, respectively. Comparing the spectra obtained for the ANFO produced on the basis of the P1–P5 fuel oils with the ANFO sample made based on the FO P6, it was concluded that the addition of the P1–P5 fuel oils to AN-PP practically had no impact on the structure of the studied materials. The bands connected with the presence of oils probably overlapped with the bands resulting from

the skeleton vibrations of ammonium nitrate. The presence of weak signals in the bands of 2921 cm^{-1} and 2854 cm^{-1} might indicate the occurrence of tensile vibrations of the –CH2- and –CH3- groups from the added oil [53–56].

On the basis of the conducted XRD studies, it was confirmed that at a temperature of 25 °C, all tested materials contained crystalline ammonium nitrate in a rhombic form and with a Pmmm symmetry, two particles per unit cell, and the C2v symmetry class, both for NH$_4$$^+$ and NO$_3$$^-$ [56,57]. The addition of the P1–P6 oils to ammonium nitrate (V) led to changes in the intensity of most signals induced by the ammonium nitrate, with no shifts in the position with respect to the 2Theta angle, Figure 2. The changes in the intensity of the reflections result from a varied orientation of oil particles concerning particular lattice planes, identified by the respective signals.
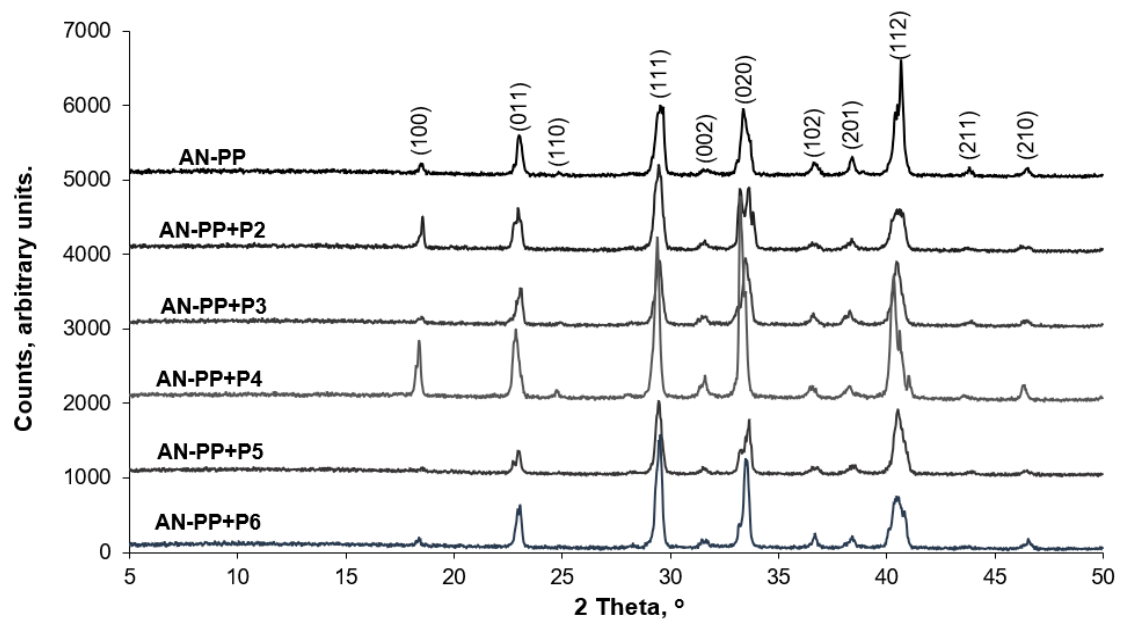

Figure 2. The XRD patterns of the ANFO obtained by mixing AN-PP with a fuel sample: P2–P6.

On the surfaces of the AN-PP granules, the presence of numerous cracks and macro-pores was observed. Both the addition of the reference fuel oil (P6) and the less viscous post-pyrolysis fuel oils (P1–P5) led to the filling of the cracks and corrugations of the structure (Figure 3a–f). The leakage of the P1–P5 oils from inside the AN-PP granules was not observed, which is usually the case when less viscous flammable components are added to AN-PP. When comparing the morphology of the non-ideal explosives samples (Figure 3a–e) with the index ANFO (Figure 3f) at *350x* magnification, no other influence of the analyzed oils on the morphology of AN-PP granules was observed.

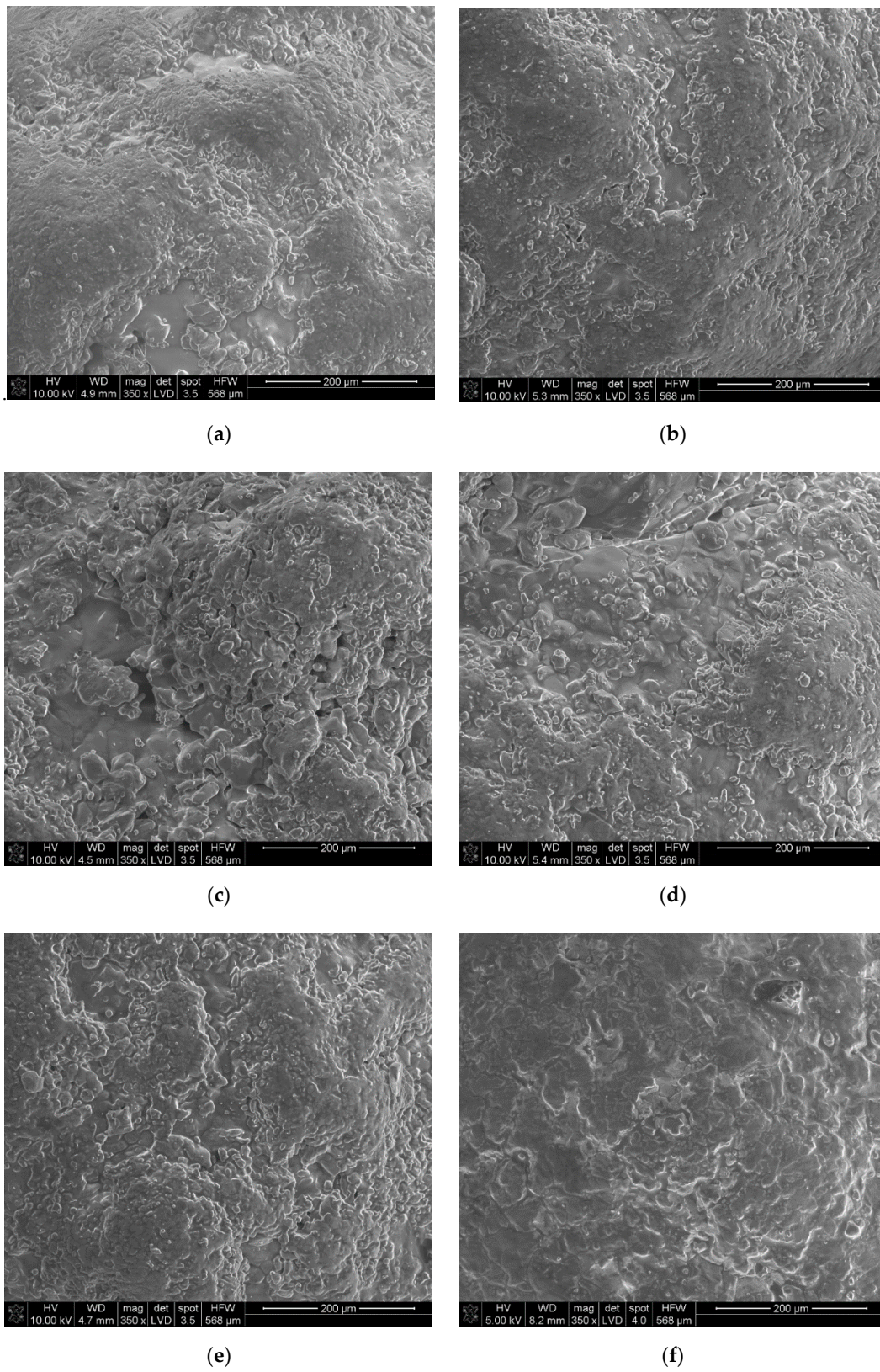**Figure 3.** The results of an SEM analysis for the ANFO obtained by mixing with oil: (**a**) P1, (**b**) P2, (**c**) P3, (**d**) P4, (**e**) P5, and (**f**) P6.

3.3. Blasting Tests

On the basis of the detonations of the produced ANFO samples, the explosion energy was determined to be within the range of 3950–4020 J·g^{-1} (Table 4). Despite the continuous addition of the feed material to the pyrolysis process, similar detonation energies were observed. The fluctuation of the energy was influenced by the chemical composition of fuel oil samples. Plastic addition influences the hydrogen and carbon content, which has an impact on the heat of combustion. Another factor that should be taken under consideration is the density of the non-ideal explosives. However, this influence is discussed further. It should be highlighted that due to the possible solidification of the re-use fuel oil (FO sample P1–P5) in normal conditions, the high content of hydrocarbons (>C15) was broken down through atmospheric distillation. This results with a possible decrease of the heat of explosion, which should be explained by the influence on carbon and hydrogen content in the fuel oil chemical composition. This was confirmed by the [21] and [56].

By comparing the energy values for particular samples with the explosion energy of the reference sample (AN-PP mixed with FO sample P6) (3940 J·g^{-1}) it was found that, regardless of their chemical composition, the tested oils could be an alternative to conventional combustible components used for the manufacturing of ANFO.

The measurements of the velocity of detonation revealed that ANFO based on the re-use FO had an average VOD within the range of ca. 2510–2590 m·s^{-1}, Table 5. In comparison with the index ANFO (ANFO based on P6 FO sample, 3140 m·s^{-1}), non-ideal explosives that were based on the re-use FO had a lower VOD. However, the obtained VOD showed that non-ideal explosives based on re-use FO could be applied in typical blasting work performed in hard resistance rock masses. The fluctuation of the velocity of detonations of non-ideal explosive based on the pyrolysis derived fuel oil could be explained by the differing content of different types of plastic. Based on Table 5, it could be concluded that with an increase of explosive density, the VOD rises; Figure 4. The Chapman-Jouguet theory can explain this example. Chapman-Jouguet assumed that between unreacted explosives and completely reacted gaseous products there is a steady-state detonation condition (where the Rayleigh line is tangent with the Hugoniot's detonation products line).
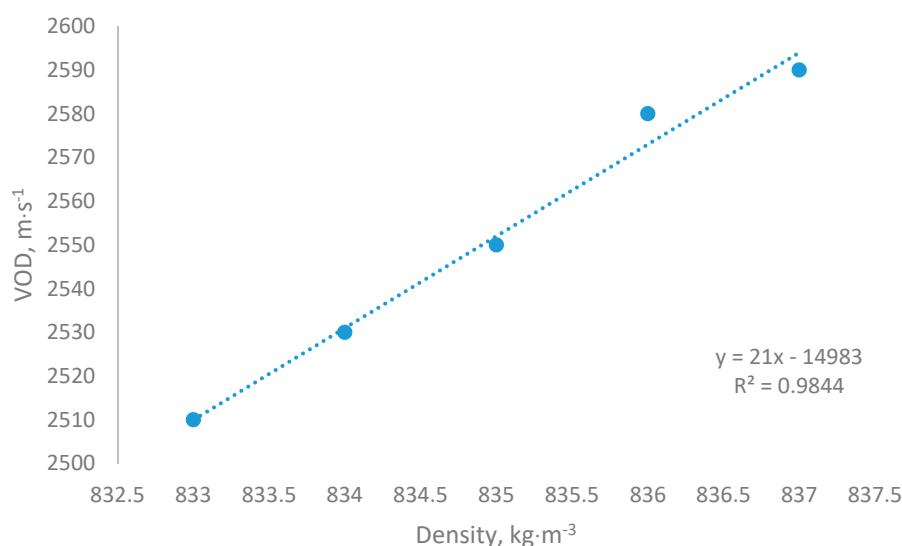

Figure 4. Relation between ANFO's VOD and density.

Moreover, the conservation of mass and momentum equations, which are called the Hugoniot equations, describe that an equilibrium state is dependent on the explosive material density or density of gaseous products [58,59]. However, it should be pointed out that ANFO is a non-ideal explosive. In that case, the shock front is always curved, and the flow of gaseous products diverges. This means that a chemical reaction is never completed in the detonation zone. Byers-Brown indicated that the detonation driving zone

terminates at the sonic line and contributes to the support of the detonation process [60]. As a result of the non-ideal detonation, the explosive VOD might approach but never exceed the ideal detonation velocity.

Based on Figure 5, it can be observed that with an increase of VOD, the heat of explosion rises. This can probably be explained by the appearance of hot spots and heat loss during the detonation process. In case of ANFO, the charge density can be influenced by the fuel oil (minor influence due to the low content of FO in ANFO composition, as well as similar density to AN-PP) and ammonium nitrate (V) (major influence due to high weight ratio in ANFO composition and similar density to FO). In the case of non-ideal explosive samples based on the re-use fuel oils, it can be observed that the density was influenced by the fuel oil. The density of the fuel oil depended on the plastic content. It can be assumed that the addition of a specific assortment of plastic improved the balance between carbon and hydrogen, which resulted in improving the heat of combustion. Probably in the case of plastic addition, the more dense FO samples had a higher heat of combustion, which resulted in a higher detonation temperature and heat of explosion. In the case of the oxygen component between different AN-PP assortments, the change of the density would be influenced by the transformation of the granule diameter. In such a case, with an increase of the charge density, distances between granules would be smaller. This situation indicated that the distance between hot spots should improve, which should result in a lower heat loss during the progress of the shock front and zone of the chemical reaction. The lower heat loss would improve the detonation temperature and heat of explosion.
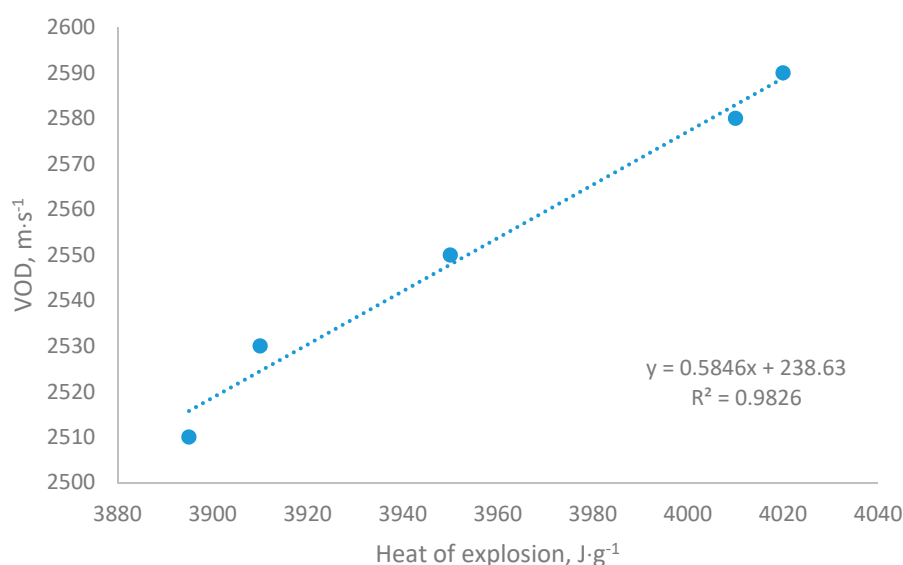

Figure 5. The relation between ANFO's VOD and heat of the explosion.

4. Conclusions

On the basis of the physicochemical analyses, it was determined that despite some differences between post-pyrolysis FOs and reference FO, post-pyrolysis FO could be applied in ANFO as the flammable component, once FO met an additional requirement. In the case of the P1–P5 oils, significantly lower flashpoints (approximately 59.4–62.2 °C) were obtained in comparison with the flashpoint of the reference oil P6 (127.3 °C), which indicated the risk of explosion of these oils during storage. A low cloud point of post-pyrolysis oils points out to a difficulty in crystallization, which increases their applicability in the manufacturing of emulsion explosives. Moreover, the P1–P5 oils (1.93–1.99 $mm^2 \cdot s^{-1}$), due to their low kinematic viscosity, should not cause mechanical damage (e.g., of pumps) to the currently used feeding (charging) systems. The TSI coefficient indicated that pyrolysis FO sample 5 is characterized by low stability, which indicates that additional post-processing

of the post-pyrolysis FO should be made. The post-processing should aim at decreasing the content of unsaturated hydrocarbons.

As a result of the detonations of the ANFO obtained by mixing it with pyrolysis-derived fuel oils (P1–P5), the average explosion energy that was achieved fell within the range of 3950–4020 $J \cdot g^{-1}$, and this result was close to the explosion energy of the reference sample of ANFO (3940 $J \cdot g^{-1}$). It seemed to indicate the applicability of the analyzed post-pyrolysis oils as an alternative to the currently used combustible components. Moreover, the obtained values of the heat of detonation revealed the relation between the obtained heat of explosion and charge density. This was a result of the differing hydrogen and carbon content due to the chemical composition of the tested FO.

Blasting tests showed that the non-ideal explosive based on re-use fuel oil had a lower VOD in comparison with the ANFO index sample. It was established that the velocity of detonation was influenced by the charge density, which was confirmed by numerous pieces of research. VOD fluctuations were derived from the differing content of the plastic, which was added to the pyrolysis process. Based on the obtained VOD, it can be concluded that obtained non-ideal explosives could be used for blasting works in the hard resistance rock masses.

The XRD and IR analyses confirmed the presence of oils in the obtained ANFO samples. Moreover, they showed that the tested re-use oils did not affect the explosive's morphology, which confirmed that this type of FO could be used as a flammable component. The morphological studies demonstrated that the P1–P5 oils with a lower viscosity in comparison to the reference oil did not leak from the inside of the AN-PP granules, filling their cracks and macrospores.

Author Contributions: Conceptualization, A.B.; methodology, A.B.; validation, A.B.; formal analysis, A.B.; investigation, A.B., Ł.K., D.C., M.D., M.T., J.B. and M.Z.; resources, A.B. and D.C.; writing—original draft preparation, A.B., Ł.K., D.C., M.D., M.T., J.B. and M.Z.; writing—review and editing, A.B. visualization, A.B. and Ł.K.; supervision, A.B. All authors have read and agreed to the published version of the manuscript.

Institutional Review Board Statement: Not applicable.

Informed Consent Statement: Not applicable.

Data Availability Statement: The data presented in this study are available on request from the corresponding author (A.B.). The data are not publicly available due to restrictions which include information that could compromise the privacy of research participant.

Conflicts of Interest: The authors wish to confirm that there are no known conflict of interest associated with this publication and there has been no significant financial support for this work that could have influenced its outcome.

References

1. Maranda, B.; Gołąbek, J.; Kasperski, J. *Materiały Wybuchowe Emulsyjne*; Wydawnictwo Naukowo-Techniczne: Warszawa, Poland, 2015.
2. Borowik, M.; Biskupski, A.; Dawidowicz, M.; Buczkowski, D. Rules of safe storage of the ammonium nitrate ferlitizers. *Przem. Chem.* **2013**, *92*, 2148–2152.
3. Biessikirski, A.; Kuterasiński, Ł.; Dworzak, M.; Pyra, J.; Twardosz, M. Comparison of structure, morphology and topography of fertilizer-based explosives applied in the mining industry. *Microchem. J.* **2019**, *144*, 39–44. [CrossRef]
4. Landucci, G.; Reniers, G.; Cozzani, V.; Salzano, E. Vulnerability of industrial facilities to attacks with imporivised devices aimed at triggering domino scenarios. *Reliab. Eng. Syst. Saf.* **2015**, *143*, 53–62. [CrossRef]
5. Biessikirski, A.; Kuterasiński, Ł. *Research on Morphology and Topology of ANFO Based on Various Types of Oxygen Component*; Wydawnictwa AGH: Krakow, Poland, 2018.
6. Miyake, A.; Takahara, K.; Ogawa, T.; Ogata, Y.; Wada, Y.; Arai, H. Influence of physical properties of ammonium nitrate on the detonation behavior of ANFO. *J. Loss Prev. Process Ind.* **2001**, *14*, 533–538. [CrossRef]

7. Maranda, A. Badanie procesu detonacji sypkich górniczych amonowo-saletrzanych mieszanin wybuchowych zawierających pył aluminiowy. *Przegląd Górniczy* **1998**, *54*, 43–49.
8. Nazarian, A.; Presser, C. Forensic methodology for the thermochemical characterization of ANNM and ANFO homemade explosives. *Thermochim. Acta* **2015**, *608*, 65–75. [CrossRef]
9. Paszula, J.; Kowalewski, E. Study of the detonation development of non-ideal explosive. *Mater. Wysokoenergetyczne* **2015**, *7*, 95–105.
10. Trzciński, W.; Haque-Pawlik, H. Application of the cylinder test in determining the characteristics of non-ideal explosives. *Mater. Wysokoenergetyczne* **2016**, *8*, 13–26.
11. Zhang, Q.; Chang, Y. A predictive method for the heat of explosion of non-ideal aluminized explosives. *Cent. Eur. J. Energ. Mater.* **2013**, *10*, 541–554.
12. Sałaciński, T.; Florczak, B.; Maranda, A. Use of ammonium nitrate(V) as component of high-energy materials in Poland. *Przem. Chem.* **2013**, *92*, 2225–2228.
13. Zygmunt, B.; Buczkowski, D. Influence of ammonium nitrate prills properties on detonation velocity of ANFO. *Propellants Explos. Pyrotech.* **2007**, *32*, 411–414. [CrossRef]
14. Viktorov, S.D.; Frantov, A.E.; Lapikov, I.N.; Andreev, V.V.; Starshinov, A.V. Effect of the microstructure of ammonium nitrate granules on the detonability of composite propellants based on it. Combust. *Explos. Shock Waves* **2016**, *52*, 727–731. [CrossRef]
15. Lotspeich, E.; Petr, V. The characterization of ammonium nitrate mini-prills. In *Dynamic Behavior of Materials 319–325, Proceedings of the 2014 Annual Conference on Experimental and Applied Mechanics, Lombard, IL, USA, 3–5 June 2014*; Song, B., Casem, D., Kimberley, J., Eds.; Springer: Cham, Switzerland, 2015; Volume 1.
16. Sinditskii, V.P.; Egorshev, V.Y.; Levshenkov, A.I.; Serushkin, V.V. Ammonium nitrate: Combustion mechanism and the role of additives. *Propellants Explos. Pyrotech.* **2005**, *30*, 269–280. [CrossRef]
17. Gunawan, R.; Zhang, D. Thermal stability and kinetics of decomposition of ammonium nitrate in the presence of pyrite. *J. Hazard. Mater.* **2009**, *165*, 751–758. [CrossRef] [PubMed]
18. Deribas, A.A.; Kudinov, V.M.; Matveenkov, F.I.; Simonov, V.A. Effect of initial parameters on the process of wave formation in explosive welding. *Combust. Explos. Shock Waves* **1967**, *3*, 344–348. [CrossRef]
19. Miyake, Y.; Ohtagaki, T.; Abe, Y.; Wada, Y.; Nakayama, Y.; Ogawa, T. Experimental determination of the detonation front curvature of non-ideal explosive ANFO. *Mater. Sci. Forums* **2004**, *465–466*, 181–184. [CrossRef]
20. Zygmunt, B. Detonation parameters of mixtures containing ammonium nitrate and aluminium. *Cent. Eur. J. Energ. Mater.* **2009**, *6*, 57–66.
21. Maranda, A.; Gałęzowski, D.; Papliński, A. Investigations on detonation and thermochemical parameters of aluminized ANFO. *J. Energ. Mater.* **2003**, *21*, 1–14. [CrossRef]
22. Maranda, A.; Paszula, J.; Zawadzka-Małota, I.; Kuczyńska, B.; Witkowski, W.; Nikolczuk, K.; Wilk, Z. Aluminum powder influence on ANFO detonation parameters. *Cent. Eur. J. Energ. Mater.* **2011**, *8*, 279–293.
23. Stramquist, D.M.; Wathen, B.J. Waste Products in Distillation for Glycol Products in ANFO Explosives as Replacement for Fuel Oils. U.S. Patent 5531843A, 2 July 1996.
24. Biessikirski, A.; Wądrzyk, M.; Janus, R.; Biegańska, J.; Jodłowski, G.; Kuterasiński, Ł. Study on fuel oils used in ammonium nitrate-based explosives. *Przem. Chem.* **2018**, *97*, 457–462.
25. Uçar, S.; Özkan, A.R.; Karagöz, S. Co-pyrolysis of waste polyolefins with waste motor oil. *J. Anal. Appl. Pyrolysis* **2016**, *119*, 233–241. [CrossRef]
26. Sipra, A.S.; Gao, N.; Sarwar, H. Municipal solid waste (MSW) pyrolysis for bio-fuel production: A review of effects of MSW components and catalysts. *Fuel Process. Technol.* **2018**, *175*, 131–147. [CrossRef]
27. Shie, J.; Lin, J.; Chang, C.; Shih, S.; Lee, D.; Wu, C. Pyrolysis of oil sludge with additives of catalytic solid wastes. *J. Anal. Appl. Pyrolysis* **2004**, *71*, 695–707. [CrossRef]
28. Lam, S.S.; Russell, A.D.; Lee, C.L.; Chase, H.A. Microwave-heated pyrolysis of waste automotive engine oil: Influence of operation parameters on the yield, composition, and fuel properties of pyrolysis oil. *Fuel* **2012**, *92*, 327–339. [CrossRef]
29. Gómez-Rico, M.F.; Marty´ın-Gullón, I.; Fullana, A.; Conesa, J.A.; Font, R. Pyrolysis and combustion kinetics and emissions of waste lube oils. *J. Anal. Appl. Pyrolysis* **2003**, *68–69*, 527–546. [CrossRef]
30. Hakki Metecan, I.; Ozkan, A.R.; Isler, R.; Yanik, J.; Saglam, M.; Yuksel, M. Naphtha derived from polyolefins. *Fuel* **2005**, *84*, 619–628. [CrossRef]
31. Sriningsih, W.; Garby Saerodji, M.; Trisunaryanti, W.; Triyono; Armunanto, R.; Falah, I.I. Fuel production from LDPE plastic waste over natural zeolite supported Ni, Ni-Mo, Co and Co-Mo metals. *Procedia Environ. Sci.* **2014**, *20*, 215–224. [CrossRef]
32. Al-Salem, S.M.; Antelava, A.; Constantinou, A.; Manos, G.; Dutta, A. A review on thermal and catalytic pyrolysis of plastic solid waste (PSW). *J. Environ. Manag.* **2017**, *197*, 177–198. [CrossRef]
33. Opatokun, S.A.; Strezov, V.; Kan, T. Product based evaluation of pyrolysis of food waste and its digestate. *Energy* **2015**, *92*, 349–354. [CrossRef]
34. Kabir, G.; Hameed, B.H. Recent progress on catalytic pyrolysis of lignocellulosic biomass to high-grade bio-oil and bio-chemicals. *Renew. Sustain. Energy Rev.* **2017**, *70*, 945–967. [CrossRef]
35. He, X.; Liu, Z.; Niu, W.; Yang, L.; Zhou, T.; Qin, D.; Niu, Z.; Yuan, Q. Effects of pyrolysis temperature on the physicochemical properties of gas and biochar obtained from pyrolysis of crop residues. *Energy* **2018**, *143*, 746–756. [CrossRef]

36. Undri, A.; Rosi, L.; Frediani, M.; Frediani, P. Efficient disposal of waste polyolefins through microwave assisted pyrolysis. *Fuel* **2014**, *116*, 662–671. [CrossRef]

37. Kalargaris, I.; Tian, G.; Gu, S. The utilization of oils produced from plastic waste at different pyrolysis temperatures in a DI diesel engine. *Energy* **2017**, *131*, 179–185. [CrossRef]

38. Kalargaris, I.; Tian, G.; Gu, S. Combustion, performance and emission analysis of a DI diesel engine using plastic pyrolysis oil. *Fuel Process. Technol.* **2017**, *157*, 108–115. [CrossRef]

39. Kalargaris, I.; Tian, G.; Gu, S. Experimental evaluation of a diesel engine fueled by pyrolysis oils produced from low-density polyethylene and ethylene–vinyl acetate plastics. *Fuel Process. Technol.* **2017**, *161*, 125–131. [CrossRef]

40. Owusu, P.A.; Banadda, N.E.; Zziwa, A.; Seay, J.; Kiggundu, N. Reverse engineering of plastic waste into useful fuel products. *J. Anal. Appl. Pyrolysis* **2018**, *130*, 285–293. [CrossRef]

41. Phung, T.K.; Casazza, A.A.; Perego, P.; Capranica, P.; Busca, G. Catalytic pyrolysis of vegetable oils to biofuels: Catalyst functionalities and the role of ketonization on the oxygenate paths. *Fuel Process Technol.* **2015**, *140*, 119–124. [CrossRef]

42. Chen, G.; Zhang, X.; Ma, W.; Yan, B.; Li, Y. Co-pyrolysis of corn-cob and waste cooking-oil in a fixed bed reactor with HY upgrading process. *Energy Procedia* **2014**, *61*, 2363–2366. [CrossRef]

43. Mahari, W.A.W.; Chong, C.T.; Lam, W.H.; Nyuk, T.N.S.T.A.; Moh, L.M.; Ibrahim, D.; Lama, S.S. Microwave co-pyrolysis of waste polyolefins and waste cooking oil: Influence of N_2 atmosphere versus vacuum environment. *Energy Convers. Manag.* **2018**, *171*, 1292–1301. [CrossRef]

44. PN-EN ISO 3675:2004. *Ropa Naftowa i Ciekłe Przetwory Naftowe. Laboratoryjne Oznaczanie Gęstości*; PKN: Warszawa, Poland, 2004.

45. PN-EN ISO 3104:2004. *Przetwory Naftowe. Ciecze Przezroczyste i Nieprzezroczyste. Oznaczanie Lepkości Kinematycznej i Obliczanie Lepkości*; PKN: Warszawa, Poland, 2004.

46. ASTM D5773-20. *Standard Test Method for Cloud Point of Petroleum Products and Liquid Fuels (Constant Cooling Rate Method)*; ASTM International: West Conshohocken, PA, USA, 2020.

47. PN-ISO 3016:2019-06. *Przetwory Naftowe i Produkty Podobne Pochodzenia Naturalnego lub Syntetycznego. Oznaczanie Temperatury Płynięcia*; PKN: Warszawa, Poland, 2019.

48. ASTM D7094-17. *Standard Test Method for Flash Point by Modified Continuously Closed Cup (MCCCFP) Tester*; ASTM International: West Conshohocken, PA, USA, 2017.

49. ASTM D93-20. *Standard Test Method of Flash Point by Pensky-Martens Closed Cup Tester*; ASTM International: West Conshohocken, PA, USA, 2020.

50. Trzciński., W.; Paszula, J. On some methods of determination of the detonation energy of explosives. In Proceedings of the 9th International Seminar—New Trends in Research of Energetic Materials, Pardubice, Czech Republic, 19–21 April 2006; pp. 748–755.

51. EN 13631-14. *Explosives for Civil Uses. High Explosives. Part 14: Determination of Velocity of Detonation*; CEN: Brussels, Belgium, 2004.

52. Biessikirski, A.; Kuterasiński, Ł. Effect of the alcohol type added to ammonium nitrate on the structure and morphology of ammonium nitrate-based explosives. *Przem. Chem.* **2018**, *97*, 1718–1721.

53. Theoret, A.; Sandorfy, C. Infrared spectra and crystalline phase transitions of ammonium nitrate. *Can. J. Chem.* **1964**, *42*, 57–62. [CrossRef]

54. Biessikirski, A.; Kuterasiński, Ł.; Pyra, J.; Dworzak, M. Comparison of properties of ammonium nitrates used for production of fertilizers and explosive materials. *Przem. Chem.* **2016**, *95*, 1381–1384.

55. Wu, H.B.; Chan, M.N.; Chan, K. FTIR characterization of polymorphic transformation of ammonium nitrate. *Aerosol Sci. Technol.* **2007**, *41*, 581–588. [CrossRef]

56. Biessikirski, A.; Kuterasiński, Ł. Morphological properties of ANFO explosives obtained with the use of liquid combustibles. *Przem. Chem.* **2018**, *97*, 587–590.

57. Hendricks, S.B.; Posnjak, E.; Kracek, F.C. Molecular rotation in the solid state. The variation of the crystal structure of ammonium nitrate with temperature. *J. Am. Chem. Soc.* **1932**, *54*, 2766–2786. [CrossRef]

58. Biessikirski, A. *Research the Physiochemical Properties of Non-Ideal Explosives Based on Various Types of Ammonium Nitrate(V) and Fuel Oils*; Wydawnictwa AGH: Krakow, Poland, 2020.

59. Gotovac Atlagic, S.; Biessikirski, A.; Kuterasiński, Ł.; Dworzak, M.; Twardosz, M.; Sorogas, N.; Arvanitidis, J. On the investigation of microstructured charcoal as an ANFO blasting enhancer. *Energies* **2020**, *13*, 4681. [CrossRef]

60. Byers Brown, W. *Critical Review of Theories of Steady Non-Ideal Two-Dimensional Detonation of Condensed Explosives*; Confidential Report to HSBM Participants; Mass Action: UK, 2002.